Stresses in thin sheets at fluid interfaces

To the editor — The mechanical response of thin films and filaments at fluid interfaces is affected by elastocapillary stresses. We aim to clarify the role of the solid–fluid interfacial energy in such situations by showing that it affects the thermodynamic distribution of stresses within the solid body but not the mechanical response of the thin film to external forces.

Molecules at the surface of a condensed phase experience asymmetric interactions, giving rise to an excess energy relative to the bulk. For liquids at thermodynamic equilibrium, this leads to a decreased density near the surface, and hence an isotropic tensile stress (force per unit length) on surface molecules that is numerically equal to the surface energy (energy per unit area)[1]. Both at the surface and in the bulk, solids differ fundamentally from liquids in having a finite shear rigidity due to preferred spatial arrangements of particles whose relative distances determine a 'target metric' and corresponding stress-free configurations. Hence, when a solid is placed in contact with a liquid or vapour, its molecules do not flow, but are displaced from their preferred relative distances, which may give rise to strain. The consequent stress induced in the solid by the solid–fluid interaction has been the subject of differing points of view in the literature[2–6], which we seek to clarify in this Correspondence. Here we focus on the illustrative example of the stress in a thin, flexible solid at a fluid interface.

There has been a recent surge in designing responsive materials for applications ranging from microfluidics, soft robotics, drug delivery and tissue engineering. In many cases, the responsiveness of the material is designed to take advantage of the deformation under the capillary forces of the surrounding fluid environment; in other cases, these forces lead to elastic failure of the device. The capacity for large deformations may be imparted either by the slender geometry of filaments or films, or by material softness (using solids with low Young's moduli of a few megapascals or less). Based on an experimental example drawn from the first of these two classes, this Correspondence clarifies that the stress in the body averaged over a cross-section normal to its surface is not affected by the solid interfacial energy. This conclusion is valid for both classes of 'soft capillary' phenomena, but is particularly relevant for understanding the mechanics of thin sheets and slender filaments, as discussed later.

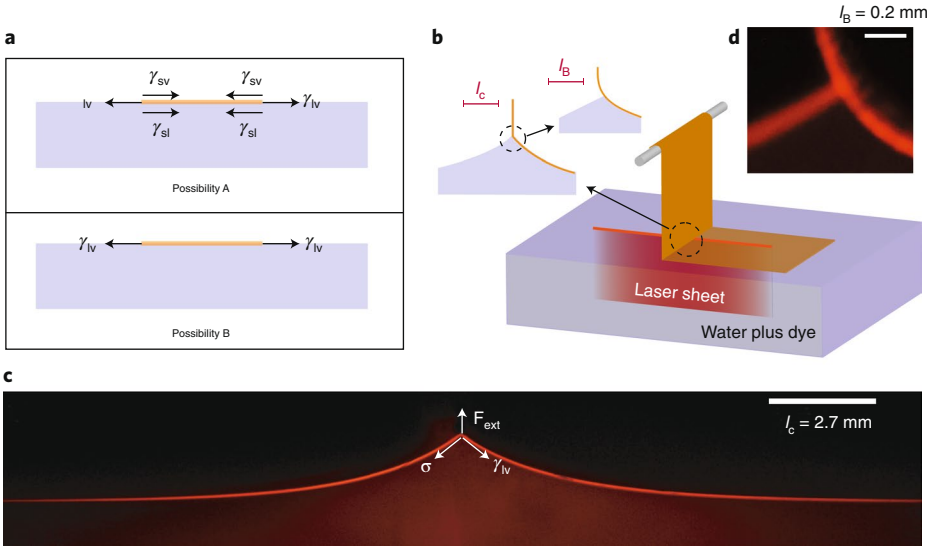

Fig. 1 | Measuring the stress in a thin film at a fluid interface. a, Two possibilities for the stress in a thin solid film floating on the surface of a liquid. Possibility A, $\sigma = \gamma_{lv} - (\gamma_{sl} + \gamma_{sv})$, and possibility B: $\sigma = \gamma_{lv}$. **b**, Schematic of the experiment. A laser-sheet-based fluorescent imaging technique is used to image the meniscus formed when one end of a rectangular film floating on the surface of water is lifted slowly to avoid any inertial effects. The film is rectangular (width × length: 60 mm × 22 mm), with one edge draped around a triangular frame (shaped like a clothes hanger) and made with graphite rods. We choose the dimensions of the sheet to greatly exceed the capillary length. The water is dyed with fluorescent dye rhodamine B at a concentration of 6.710^{-6} wt%. The insets show schematic representations of the geometry of the meniscus near the three-phase contact when viewed at two different levels of magnifications corresponding to capillary length l_c and bendo-capillary length l_B. **c**, Experimentally observed meniscus for a polystyrene film of thickness 54 nm on water surface ($l_c = 2.71$ mm). The image is taken with a Nikon 5300D-SLR camera, with a red filter corresponding to the emission peak of the dye. The camera is levelled with a precision of ~0.01° with respect to the horizontal. Forces acting at the vertex are marked; we discuss later in the Correspondence why it is legitimate to mark γ_{lv} as a stress component. Note that the menisci on the film (left of the vertex) and bare water (right of the vertex) sides appear indistinguishable. **d**, When magnified at the bendo-capillary scale l_B, shown here for a polystyrene film of thickness $t = 2$ μm, one can see the smoothly varying slope of the film near the vertex where the water–air surface (coming from the left side of the image) meets the polystyrene film.

A classic example in which one may confuse surface energy with stress is the partial wetting of a sessile drop resting on a solid surface. For a stiff solid substrate, the contact angle (θ_Y) is determined by a minimization of the total surface energy with contributions from all the three interfaces: $\cos(\theta_Y) = \frac{\gamma_{sv} - \gamma_{sl}}{\gamma_{lv}}$, where γ_{lv}, γ_{sl} and γ_{sv} characterize, respectively, the energy per unit area of the liquid–vapour, solid–liquid, and solid–vapour surfaces. This is commonly represented in the Young–Laplace–Dupré (YLD) picture as a balance between three forces acting tangentially to the three interfaces with magnitudes equal to the corresponding interfacial energies. This force-balance picture has formed the basis for analysing a wide range of elastocapillary phenomena such as the contact line at the wetting ridge formed by a sessile drop on a soft elastomeric gel[7–10] and the shape of a drop on a thin glassy polymer film[11–15]. Despite the intuitive appeal of the YLD picture, it is important to realize that the surface energies γ_{sl} and γ_{sv} should not be automatically identified with tangential stresses experienced through the solid[11,16–18].

We make explicit the distinction between surface energy and stress associated with a solid adjacent to a fluid through a simple example. Consider a thin solid film floating on a liquid: the net tangential

stress in the plane of the film (Fig. 1a) is the two-dimensional (2D) stress, denoted as σ, obtained by integrating the tangential components of the three-dimensional (3D) stress over the thickness of the film ($\sigma = \int_{-t/2}^{t/2} \sigma^{3D}(z)\mathrm{d}z$); namely, σ is the internal force exerted on a unit length in the plane of the film. The stress is isotropic in this simple arrangement, allowing us to consider it as a spatially constant scalar (under less trivial loads, σ is spatially varying and tensorial[11,16]). A natural question, which is our focus here, is how σ relates to γ_{lv}, γ_{sl} and γ_{sv}.

Figure 1a shows two possible answers to this question. The first possibility (A) is that $\sigma = \gamma_{lv} - (\gamma_{sl} + \gamma_{sv})$, inspired by the classic force-balance depiction of the YLD contact, where the underlying assumption is that the surface energies γ_{sl} and γ_{sv} give rise to compressive stresses acting to minimize the solid–vapour and solid–liquid interfacial areas, opposing the effect of the surrounding liquid–vapour interface that pulls on the edge of the film. The other possibility (B) is $\sigma = \gamma_{lv}$, which assumes that the solid surface energies do not make any net contribution to the 2D stress σ (ref. [19]). As we will show later, underlying these two options are different assumptions regarding the nature of the stress-free state of the film, of which only one can be correct.

To address this question, we perform the experiment illustrated in Fig. 1b[20]. A rectangular polymer film 60 mm wide, 22 mm long and with thickness ranging from 54 nm to 449 nm floats on a water–air interface. The film is attached along one of the wide edges to a frame that is lifted vertically above the interface. The menisci formed near the three-phase contact line are imaged at a length scale comparable to the capillary length $l_c = \sqrt{\frac{\gamma_{lv}}{\rho g}}$, where ρ is the liquid density and g is the gravitational acceleration. A typical profile measured experimentally is shown in Fig. 1c. Quite remarkably, the shapes of the menisci on the two sides are indistinguishable, though one is a bare air–water surface and the other is covered by a thin film. This immediately suggests that the state of stress on both sides is the same, as we argue in greater detail below.

The shape of a 2D liquid meniscus $y(x)$ is given by a balance between the hydrostatic pressure and the Laplace pressure: $\gamma_{lv}\kappa + \rho g y = 0$, where $\kappa = \frac{y''(x)}{\left(1+y'(x)^2\right)^{3/2}}$ is the local curvature of the surface, and y' and y'' are the first and second derivatives with respect to the horizontal coordinate x[21]. The characteristic length scale that arises out of this balance is the capillary length $l_c = \sqrt{\frac{\gamma_{lv}}{\rho g}}$. A similar equation describes a water surface covered by a solid film but the Laplace pressure now arises from the 2D stress in the film, σ, resulting in a modified capillary length $l_{cs} = \sqrt{\frac{\sigma}{\rho g}}$. We should note here that any correction to this picture due to non-zero bending rigidity, $B \sim Et^3$, where E is the Young's modulus and t the thickness of the film, is relevant only at the scale of bendo-capillary length $l_B = \sqrt{\frac{B}{\gamma_{lv}}}$. At this scale, the film has a smoothly varying slope near the vertex where the water–air surface meets the film. We illustrate this schematically in Fig. 1b and show an example in Fig. 1d where we zoom in on a polystyrene film of thickness 2 μm at its bendo-capillary scale $l_B \approx 200$ μm (see also Croll and colleagues[20]). However, for our present discussion, we focus on a scale $\gg l_B$ where bending effects can be neglected.

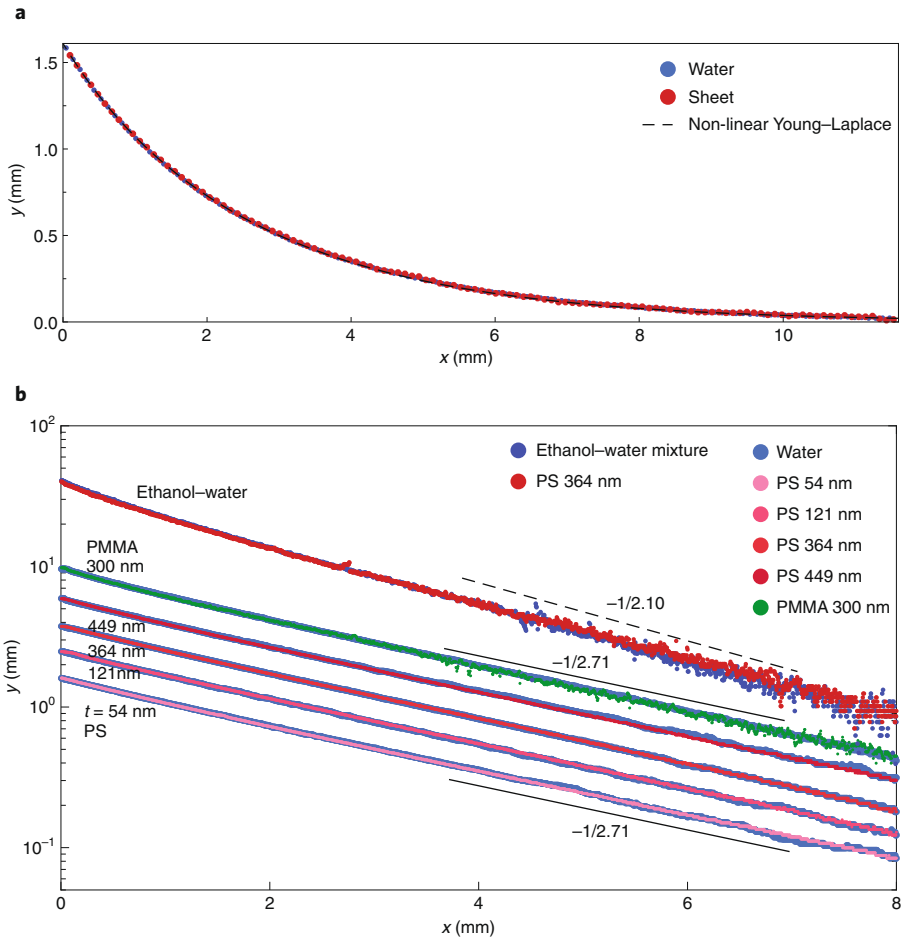

Fig. 2 | Measured meniscus profiles. Measured profiles of the meniscus, $y(x)$, on the water side (blue) and film side (red). These are plotted along with the non-linear solution of the Young–Laplace equation (black dashed line) where we use $y(0)$ from the experimental data and the capillary length of water l_c = 2.71 mm with no fit parameters. All the three plots are in excellent agreement with each other. For clarity, only every 25th data point from the experiment is plotted. **b**, Measured profiles of meniscus for polystyrene (molecular weight = 97,582 Da obtained from Polymer Source) films of various thicknesses from 54 nm to 449 nm and PMMA (molecular weight = 996,000 Da obtained from Aldrich) film of thickness 300 nm on water surface, plotted along with the corresponding menisci on the water side. Also plotted are the menisci on the two sides for a polystyrene film (t = 364 nm) on an ethanol–water (20% v/v) mixture (l_c = 2.10 mm). The straight lines are guides to the eye representing the slope $-1/l_c$. Solid lines correspond to water with l_c = 2.71 mm and the dashed line to water–ethanol mixture with l_c = 2.10 mm. As discussed in the text, γ_{sl} and γ_{sv} do not appear in any of these quantities.

In Fig. 2a, we plot the measured profiles of the menisci on both the film-covered and bare water surface. Also plotted is the full non-linear solution of the Young–Laplace equation using the capillary length of water l_c = 2.71 mm. The indistinguishability of the profiles on the two sides implies $l_{cs} = l_c$, which in turn means that $\sigma = \gamma_{lv}$. In Fig. 2b, we systematically explore this result by

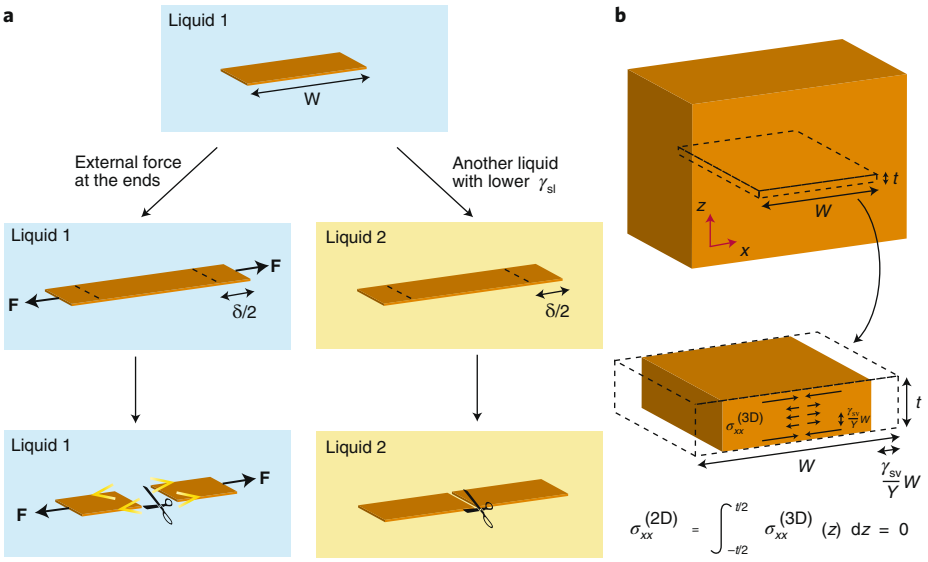

Fig. 3 | Gedankenexperiment. a, A thin film of length W completely immersed in liquid 1 is subjected to two distinct protocols. In the left panel, a force F is applied at its ends causing a strain δ/W. In the right panel liquid 1 is replaced by liquid 2, which has a lower γ_{sl} such that the film extends by the same amount δ. Although in both cases the film ends up having identical lengths, it is under stress in the left panel and is free of 2D stress in the right panel. The difference in the states of stress is easily revealed if the films are cut along their centres, causing the sheet under stress to spring apart and separate. **b**, A thin film of width W and thickness t, initially part of a large bulk, is taken out in to air. Due to its surface energy γ_{sv} the film contracts by an amount $\frac{2\gamma_{sv}}{Y}W$. Although the volumetric stress varies across the thickness of the film, being compressive at the surface and slightly tensile in the interior, the 2D stress obtained as thickness-integrated volumetric stress is zero.

varying the bending modulus, the solid surface energy, and the liquid–vapour surface energy. To test the dependence on bending rigidity we repeat the experiment with polystyrene films of various thicknesses corresponding to a 1,000-fold variation in bending rigidity. The dependence on solid interfacial energy is tested using a poly(methylmethacrylate) (PMMA) film of thickness $t = 300$ nm on the water surface. We also replaced water as the sub-phase with 20%(v/v) ethanol–water mixture with capillary length $l_c = 2.10$ mm. In all cases, we find that the meniscus profile on the film side is identical to that on the bare liquid side and is fully described by the Young–Laplace equation with the capillary length corresponding to the sub-phase. We conclude that possibility B in Fig. 1a is correct — the 2D stress in the floating film is equal to γ_{lv} with no contributions from the solid surface energies γ_{sl} and γ_{sv}.

To make sense of this result we recall that for a solid, the state of stress must be characterized with respect to a stress-free reference state. We illustrate this conceptual point through a gedankenexperiment. Starting with a thin film of length W immersed completely in liquid, we imagine two different experiments. In the first case (left panel of Fig. 3a), we apply a force F at the edges to cause a strain δ/W in the film. This results in an average 2D stress $\sigma = \frac{Y\delta}{W}$ in the film, where $Y = Et$ is the stretching modulus of the film. In the second case, we replace the surrounding liquid (1) with another liquid (2), where $\gamma_{sl_2} < \gamma_{sl_1}$, such that the film undergoes the same overall extension δ that it experienced under the force F. Here the edges of the film are free, and the new expanded configuration is the 2D stress-free reference state of the film. Cutting the film has different results in these two cases (bottom of Fig. 3a): in one case the boundary force F is now unbalanced on the two pieces of film, whereas in the other case, the two pieces are in equilibrium. This demonstrates that the film can have the same extension in comparison to the original stress-free state and, yet, in one case be under stress, and in the other case can adopt a new stress-free configuration. An important lesson to draw from this example is that there is no unique stress-free configuration for a solid object, and that the stress-free configuration depends on thermodynamic conditions. Thus, the effect of surface energy is similar to swelling or thermal expansion in that it changes the 2D stress-free configuration[22].

While surface energies do not affect the 2D stress, they do affect the distribution of the 3D stress across the thickness of the film. This is illustrated in Fig. 3b, where we consider a thin film that initially was in the interior of a bulk material and is now taken out into air. Due to the higher surface energy in air the film contracts by an amount $\frac{2\gamma_{sv}}{Y}W$. The point to note is that in describing the mechanics of films or filaments, we integrate out deformations across the thickness and account for their energetic effects through effective bending and stretching moduli. In this description, the contracted film (Fig. 3b, bottom) defines a new stress-free reference state. The volumetric stress inside the film, σ^{3D}, varies across the thickness, but its integral vanishes to give a zero 2D stress, $\sigma = \int_{-t/2}^{t/2} \sigma^{3D}(z)dz = 0$. One may wish to interpret an integral of σ^{3D}over a small depth close to the surface (for example, $\frac{\gamma_{sv}}{E} \ll t$) as a 'surface stress'; however, it has no effect as long as the relevant mechanics is governed by σ, as in the examples above.

While we showed that the net tangential stress within the film does not depend on the solid surface energies, the difference $\gamma_{sl} - \gamma_{sv}$ does affect the height of the meniscus and the angle ϕ at the vertex. When in balance with the vertical force, F_{ext}, the angle at the vertex, ϕ, observed at the scale of the capillary length, satisfies $F_{ext} = 2\gamma_{lv}\cos\left(\frac{\phi}{2}\right)$. In the YLD picture, $F_{ext} = \gamma_{lv}(1 + \cos\theta_Y)$, and thus depends only on the difference $\gamma_{sv} - \gamma_{sl}$ (we are currently studying the slow dynamics of relaxation of the vertex towards force balance).

The surface energies of solids thus play a crucial role in determining stress-free configurations in a diverse set of phenomena involving slender solids in contact with liquid phases: the spontaneous wrinkling in graphene films[23], the 'pre-stress' states in thin suspended[14] or floating films[11], blisters caused in coatings on solid surface by a thin liquid layer[24], spontaneous curling of nanoparticle ribbons[25], capillary deformation of soft rods[26] immersed in liquids, and the Shuttleworth effect in elastomeric films[6]. However, one must recall that in these problems, as in our example, solid surface energies do not contribute to the 2D stress. Consider a sessile liquid drop resting on a thin floating[11] or free-standing film[12,14,15,27]. The data and discussion presented in this Correspondence conclusively establish that the 2D stress in the film, before the drop is placed on it, is independent of the solid surface energies and depends only on the external forces, such as the surface tension of the liquid bath or mechanical clamping at the edges of the film.

This message is of topical relevance for studies of graphene oxide and other 2D solids that have been proposed as candidates for interfacial materials[28]. In characterizing the behaviour of such a film at an interface, it is tempting to use a Langmuir trough to obtain a 'surface pressure' that depends on areal coverage, akin to the characterization of a thermodynamic equation of state in molecular or particulate surfactants. In addition to the known challenges of associating stress in a solid film with the force measured by a Wilhelmy plate[29], our Correspondence clarifies that any deviation of the stress in a floating film (or assembly of films) from the isotropic liquid–vapour surface tension does not reflect a solid surface energy, but only the loading exerted on the edges of the film by the specific force apparatus.

We note that when one face of a film is attached to a rigid support, the physics cannot be described by slender body mechanics, but requires the full 3D stress distribution, even though the film itself is thin. For example, the formation of a wetting ridge[7,30] or the development of surface creasing[31], cannot be described as 2D, slender-body deformations, but rather imply a non-trivial deformation that varies across the thickness of the solid film. Thus, such examples of elastocapillary phenomena where 3D effects are significant, are settings in which the individual values of the solid surface energy, γ_{sv} and γ_{sl} (rather than merely their difference) can have a physical effect.

Data availability

Source data for Fig. 2 are provided with the paper. All remaining data are available from the authors upon request. ❐

Deepak Kumar[1,2,3], Thomas P. Russell[2,4,5,6], Benny Davidovitch[1] and Narayanan Menon[1]✉

[1]*Department of Physics, University of Massachusetts, Amherst, MA, USA.* [2]*Polymer Science and Engineering Department, University of Massachusetts, Amherst, MA, USA.* [3]*Indian Institute of Science Education and Research, Bhopal, India.* [4]*Materials Sciences Division, Lawrence Berkeley National Laboratory, Berkeley, CA, USA.* [5]*Beijing Advanced Innovation Center for Soft Matter Science and Engineering, Beijing University of Chemical Technology, Beijing, China.* [6]*Advanced Institute for Materials Research, Tohoku University, Sendai, Japan.*

✉*e-mail: menon@physics.umass.edu*

Published online: 16 April 2020

https://doi.org/10.1038/s41563-020-0640-9

References

1. Gurney, C. Surface tension in liquids. *Nature* **160**, 166–167 (1947).
2. Shuttleworth, R. The surface tension of solids. *Proc. Phys. Soc. A* **63**, 444–457 (1950).
3. Gurtin, M. E. & Murdoch, A. I. A continuum theory of elastic material surfaces. *Arch. Ration. Mech. Anal.* **57**, 291–323 (1975).
4. Makkonen, L. Misconceptions of the relation between surface energy and surface tension on a solid. *Langmuir* **30**, 2580–2581 (2014).
5. Müller, P., Saùl, A. & Leroy, F. Simple views on surface stress and surface energy concepts. *Adv. Nat. Sci. Nanosci. Nanotechnol.* **5**, 013002 (2013).
6. Schulman, R. D., Trejo, M., Salez, T., Raphaël, E. & Dalnoki-Veress, K. Surface energy of strained amorphous solids. *Nat. Commun.* **9**, 982 (2018).
7. Style, R. et al. Universal deformation of soft substrates near a contact line and the direct measurement of solid surface stresses. *Phys. Rev. Lett.* **110**, 066103 (2013).
8. Style, R. W., Hyland, C., Boltyanskiy, R., Wettlaufer, J. S. & Dufresne, E. R. Surface tension and contact with soft elastic solids. *Nat. Commun.* **4**, 2728 (2013).
9. Xu, Q. et al. Direct measurement of strain-dependent solid surface stress. *Nat. Commun.* **8**, 555 (2017).
10. Style, R. W., Jagota, A., Hui, C.-Y. & Dufresne, E. R. Elastocapillarity: surface tension and the mechanics of soft solids. *Annu. Rev. Condens. Matter Phys.* **8**, 99–118 (2017).
11. Schroll, R. D. et al. Capillary deformations of bendable films. *Phys. Rev. Lett.* **111**, 014301 (2013).
12. Schulman, R. D. & Dalnoki-Veress, K. Liquid droplets on a highly deformable membrane. *Phys. Rev. Lett.* **115**, 206101 (2015).
13. Schulman, R. D., Ledesma-Alonso, R., Salez, T., Raphaël, E. & Dalnoki-Veress, K. Liquid droplets act as "compass needles" for the stresses in a deformable membrane. *Phys. Rev. Lett.* **118**, 198002 (2017).
14. Nadermann, N., Hui, C.-H. & Jagota, A. Solid surface tension measured by a liquid drop under a solid film. *Proc. Natl Acad. Sci. USA* **110**, 10541–10545 (2013).
15. Fortais, A., Schulman, R. D. & Dalnoki-Veress, K. Liquid droplets on a free-standing glassy membrane: deformation through the glass transition. *Eur. Phys. J. E* **40**, 69 (2017).
16. Davidovitch, B. & Vella, D. Partial wetting of thin solid sheets under tension. *Soft Matter* **14**, 4913–4934 (2018).
17. Makkonen, L. Young's equation revisited. *J. Phys. Condens. Matter* **28**, 135001 (2016).
18. Gao, L. & McCarthy, T. How Wenzel and Cassie were wrong. *Langmuir* **23**, 3762–3765 (2007).
19. Bico, J., Reyssat, E. & Roman, B. Elastocapillarity: when surface tension deforms elastic solids. *Annu. Rev. Fluid Mech.* **50**, 629–659 (2018).
20. Twohig, T., May, S. & Croll, A. B. Microscopic details of a fluid/thin film triple line. *Soft Matter* **14**, 7492–7499 (2018).
21. de Gennes, P.-G., Brochard-Wyart, F. & Quéré, D. *Capillarity and Wetting Phenomena: Drops, Bubbles, Pearls, Waves* (Springer, 2013).
22. Efrati, E., Sharon, E. & Kupferman, R. Elastic theory of unconstrained non-euclidean plates. *J. Mech. Phys. Solids* **57**, 762–775 (2009).
23. Deng, S. & Berry, V. Wrinkled, rippled and crumpled graphene: an overview of formation mechanism, electronic properties, and applications. *Mater. Today* **19**, 197–212 (2016).
24. Chopin, J., Vella, D. & Boudaoud, A. The liquid blister test. *Proc. R. Soc. Lond. A* **464**, 2887–2906 (2008).
25. Pham, J. T. et al. Highly stretchable nanoparticle helices through geometric asymmetry and surface forces. *Adv. Mater.* **25**, 6703–6708 (2013).
26. Mora, S. et al. Solid drops: large capillary deformations of immersed elastic rods. *Phys. Rev. Lett.* **111**, 114301 (2013).
27. Liu, T. et al. Interaction of droplets separated by an elastic film. *Langmuir* **33**, 75–81 (2017).
28. Cote, L. J. et al. Graphene oxide as surfactant sheets. *Pure Appl. Chem.* **83**, 95–110 (2010).
29. Witten, T. A., Wang, J., Pocivavsek, L. & Lee, K. Y. C. Wilhelmy plate artifacts in elastic monolayers. *J. Chem. Phys.* **132**, 046102 (2010).
30. Shanahan, M. E. R. & de Gennes, P.-G. Equilibrium of the triple line solid/liquid/fluid of a sessile drop. In *Adhesion 11* (ed. Allen, K. W.) 71–81 (Springer, 1987).
31. Cai, S., Chen, D., Suo, Z. & Hayward, R. C. Creasing instability of elastomer films. *Soft Matter* **8**, 1301–1304 (2012).

Acknowledgements

We gratefully acknowledge financial support through the Keck Foundation, NSF-DMR 1507650, 1905698 (NM), NSF-CAREER DMR 1151780 (D.K., B.D.), NSF-DMR 1822439 (B.D.), and the Army Research Office under W911NF-17-1-0003 (T.P.R.). We thank J. D. Paulsen for useful discussions.

Author contributions

D.K., T.P.R., B.D. and N.M. contributed to the overall concept of the study. D.K. and N.M. contributed to experimental design. D.K. took the data. D.K., B.D. and N.M. contributed to data analysis. B.D. conceived the gedankenexperiment in Fig. 3. All authors contributed to writing and editing the manuscript.

Competing interests

The authors declare no competing interests.

Additional information

Supplementary information is available for this paper at https://doi.org/10.1038/s41563-020-0640-9.